

Optimization of the poro-serrated trailing edges for airfoil broadband noise reduction

Tze Pei Chong^{a)} and Elisa Dubois

Department of Mechanical, Aerospace and Civil Engineering, Brunel University London, Uxbridge, UB8 3PH, United Kingdom

(Received 29 December 2015; revised 29 July 2016; accepted 7 August 2016; published online 29 August 2016)

This paper reports an aeroacoustic investigation of a NACA0012 airfoil with a number of poro-serrated trailing edge devices that contain porous materials of various air flow resistances at the gaps between adjacent members of the serrated-sawtooth trailing edge. The main objective of this work is to determine whether multiple-mechanisms on the broadband noise reduction can co-exist on a poro-serrated trailing edge. When the sawtooth gaps are filled with porous material of low-flow resistivity, the vortex shedding tone at low-frequency could not be completely suppressed at high-velocity, but a reasonably good broadband noise reduction can be achieved at high-frequency. When the sawtooth gaps are filled with porous material of very high-flow resistivity, no vortex shedding tone is present, but the serration effect on the broadband noise reduction becomes less effective. An optimal choice of the flow resistivity for a poro-serrated configuration has been identified, where it can surpass the conventional serrated trailing edge of the same geometry by achieving a further 1.5 dB reduction in the broadband noise while completely suppressing the vortex shedding tone. A weakened turbulent boundary layer noise scattering at the poro-serrated trailing edge is reflected by the lower-turbulence intensity at the near wake centreline across the whole spanwise wavelength of the sawtooth.

© 2016 Author(s). All article content, except where otherwise noted, is licensed under a Creative Commons Attribution (CC BY) license (<http://creativecommons.org/licenses/by/4.0/>).
[<http://dx.doi.org/10.1121/1.4961362>]

[JFL]

Pages: 1361–1373

I. INTRODUCTION

Engine jet noise used to be the major noise source for a civil aircraft. However, its dominance in aviation noise has been less significant since the introduction of a high bypass ratio aero-engine. Nowadays, noise generated at the trailing edge of engine fan blades, or the airframe's high lift devices, has become more important. The noise mechanism here is related to the scattering of turbulent energy in the boundary layer into noise at the trailing edge. At high Reynolds numbers, the boundary layer that develops over the airfoil surface is turbulent and hence the radiated noise from the trailing edge is largely broadband in nature. The increase in air traffic leads to more frequent noise events to which airport neighbors are exposed to. The concern on the aircraft noise thus represents an important constraint on maintaining the growth in capacity of the airport transport system.

Another industrial application that utilizes fan blades at a high Reynolds number is the wind turbine, where trailing edge noise is also one of the dominant noise sources. The swishing noise from a wind turbine blade is produced by the combination of trailing edge noise and Doppler amplification effect of the blade movement.¹ This swishing noise can be heard at a considerable distance, especially at low frequencies where atmospheric attenuation is not very effective. This important environmental impact is one of the main reasons for the high rate of refusal to grant planning permission

for an onshore wind farm in many countries. Therefore, for the aero-engine, airframe, and wind turbine industries, it is important to invent new or further develop existing technologies to address the trailing edge noise problem.

Corrugating the trailing edges of a fan blade in the form of serration is one of the promising methods to reduce trailing edge turbulent broadband noise.^{2–7} This passive method has been demonstrated experimentally to achieve reduction of the trailing edge turbulent broadband noise level up to 8 dB.⁵ Serrated trailing edge is also effective in suppressing boundary layer instability tonal noise, where 20 dB in the overall sound pressure level reduction has been demonstrated.⁸ Except in the works by Chong and Joseph⁸ and Chong *et al.*,⁹ most of the serrations have been formed from thin flat plates, which are inserted into the trailing edge of the main airfoil body. This was done for ease of manufacture and, more importantly, to prevent vortex shedding arising from bluntness caused by cutting the serrations into the airfoil main body. However, serrated flat plate inserts are unlikely to have the structural integrity for continuous operation at high loading configuration. Moreover, introducing flat plate inserts alters the airfoil geometry and hence the global circulation around the airfoil is likely to be different from the original airfoil. Another shortcoming of a flat plate serration is that the noise performance is susceptible to misalignment between the incoming flow angle and the serration flap angle.⁵ It is also observed by Oerlemans *et al.*³ and Gruber⁵ that flat plate serration can cause an increase in noise level at high frequency. All these factors could

^{a)}Electronic mail: t.p.chong@brunel.ac.uk

potentially prevent the eventual and widespread adoption of serration technology in the aircraft and wind turbine industries.

More preferable from the points of view of structural integrity and preserving the airfoil shape is to cut the serration patterns directly into the airfoil body. This configuration is henceforth referred to “nonflat plate serration.” As shown in Fig. 1(a), a nonflat plate serration can leave a certain degree of bluntness (ϵ) on the sawtooth gaps. However, while the nonflat plate serration has also been shown to afford a good level of broadband noise reduction across a wide frequency range,⁹ the overall noise reduction is compromised by a high level of bluntness-induced narrowband vortex shedding noise predominantly at a lower frequency. Previous attempts at reducing the bluntness-induced vortex shedding by wrapping a woven-wire mesh screen around the nonflat plate serrated trailing edge was only partially successful.¹⁰ The reason might be due to the low pressure drop coefficient of the mesh screen ($K = 1.5$) and its incapability to suppress the vortex shedding effectively. The mesh screen also seems to affect the serration negatively for the reduction of broadband noise. Moreover, noise level is found to increase at high frequency due to the surface roughness introduced by the mesh screen to the sawtooth surface. As a result, the overall noise performance is not improved much.

A more effective approach to introduce serrations directly into the main body of airfoil is the “poro-serrated”

concept,¹¹ which utilizes porous foams or brushes between adjacent members of the sawtooth to fill the air gap. As shown in Fig. 1(b), the porous foams were cut precisely to match the exact volume and shape of the sawtooth gaps, so that an original airfoil profile throughout the chord length is preserved. While the porous foam at the sawtooth gaps has been shown to completely suppress the vortex shedding, significant turbulent broadband noise reduction can simultaneously be achieved. The paper also reports that for airfoil with poro-serrated trailing edge, the lift and drag coefficients at the pre-stall regime remain largely the same performance as the baseline, straight trailing edge case.

So far, there is no general consensus regarding the exact mechanism of turbulent broadband noise reduction by a trailing edge serration. Theoretical approaches^{12,13} describe the obliqueness of the sawtooth edges as an effective geometry to reduce the coherences between the acoustic sources, and cause a phase shift in acoustic radiation along the wetted edge. Broadband noise reduction is therefore achieved through the destructive acoustical interference of these different scattering sources. Results of an experimental study¹⁴ on turbulent flow over a flat plate with a serrated sawtooth trailing edge demonstrate that the wall pressure power spectral density (PSD) and the spanwise coherence remain largely unchanged over a large area of the sawtooth. However, they also observed a strong presence of pressure-driven oblique vortical structures near the sawtooth side edges, where they interact with the turbulent boundary layer and cause a redistribution of the momentum transport and turbulence energy. It has been suggested that the vortical structure will affect the acoustical scattering along the sawtooth oblique edges that eventually results in broadband noise reduction. However, further investigation is still needed to ascertain this.

It has also been demonstrated that turbulent broadband noise can be reduced when the whole trailing edge is made from porous materials.^{15–18} The underpinning mechanism is perhaps more straightforward than the serration case. The porous nature of the material allows communication between flow on the upper and lower sides of the airfoil, thus reducing the acoustical dipole strength at the trailing edge. One of the important parameters to describe a porous material is the air flow resistivity, which is related to the amount of pressure drop across a porous material. Generally speaking, the level of the radiated broadband noise will be lower if the trailing edge has a low-flow resistivity so that transverse flow is likely to be initiated by through-flow at the porous medium near the trailing edge.

In the poro-serrated configuration, the main mechanism underpinning the broadband noise reduction is primarily associated with the serration geometry.¹¹ Although the porous material in this configuration is originally intended to eliminate the vortex shedding, the results in Vathylakis *et al.*¹¹ show that it also has a potential to contribute in further broadband noise reduction. It is therefore hypothesized that the poro-serrated trailing edge could offer further reduction in the turbulent broadband noise level.

The main objective of this work is to investigate whether multiple-broadband noise reduction mechanisms can co-exist in the poro-serrated trailing edge configuration.

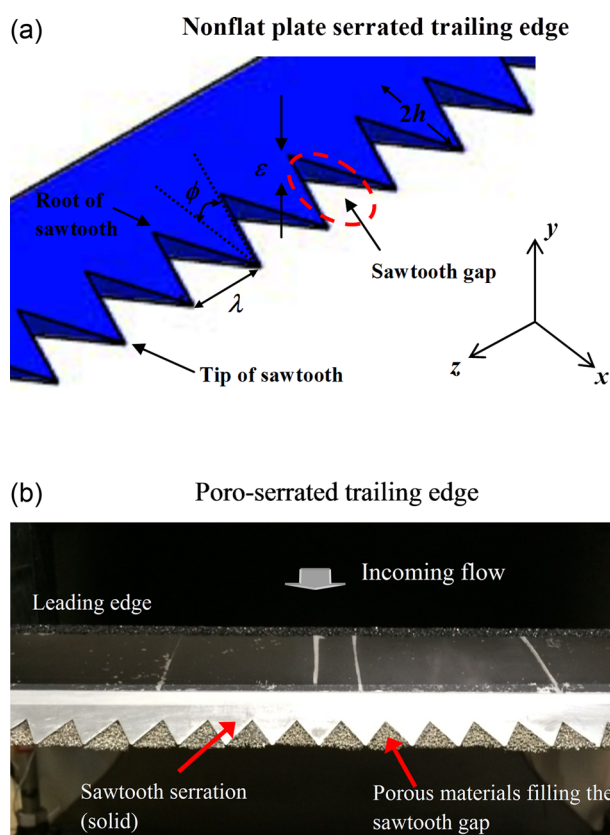


FIG. 1. (Color online) (a) Parameters associated with a nonflat plate type sawtooth geometry: serration angle (ϕ), serration amplitude ($2h$), serration wavelength (λ), and root bluntness (ϵ), (b) photograph of a poro-serrated trailing edge installed on a NACA0012.

By utilizing the same serration geometry throughout the noise experiments, several porous materials that produce different flow resistivities were used to fill the sawtooth air gaps. The investigation also includes the nonflat plate configuration that comprises the same serration geometry but without the porous materials at the sawtooth air gaps.

II. EXPERIMENTAL SETUP

To be consistent with our previous works,^{8–11} the airfoil under investigation is a NACA0012 airfoil with a sawtooth serration cut directly into the main body of the airfoil. The chord length (C) of the airfoil is 0.15 m, and the width is 0.3 m. Between the leading edge $x/C = 0$, and $x/C = 0.79$, the original NACA0012 airfoil profile is unmodified, where x is the streamwise direction. Further downstream, $0.79 \leq x/C \leq 1.0$, is a section that can be removed and replaced by either an unmodified or modified trailing edge profile. Once attached, the trailing edge section forms a continuous profile giving the appearance that the serrations are cut into the main body of the NACA0012 airfoil. Turbulators were applied at $0.15 C$ from the leading edge, and on both sides of the airfoil, in order to ensure that turbulent boundary layers are generated before reaching the trailing edge. Figure 1(a) shows the parameters associated with a nonflat plate serrated trailing edge geometry. Typical parameters include the serration amplitude $2h$ (longitudinal distance from sawtooth tip to root), serration wavelength λ (spanwise distance from sawtooth tip to tip), and serration angle ϕ . A prominent feature for this type of serrated trailing edge is the exposure of a significant bluntness (ε) at the root region, which would otherwise be negligible for the conventional flat plate type serrated trailing edge. A schematic for a poro-serrated trailing edge is shown in Fig. 1(b). As mentioned previously, the porous material was cut precisely to follow the volume and shape of each sawtooth gap to ensure that a continuous airfoil profile is maintained.

Table I summarizes the geometrical parameters of the trailing edge devices investigated in this study. To make it easier to differentiate the trailing edge devices, they are named according to the values of their serration angle ϕ , and flow resistivity σ at the sawtooth gaps. For example, a poro-serrated trailing edge that has a serration angle of 10° and flow resistivity of 2.5 kN s m^{-4} will be named as $\phi_{10}\sigma_{2.5k}$. Likewise, a nonflat plate serrated trailing edge that also has a

serration angle of 10° , but naturally without flow resistance at the sawtooth gaps, will be named as $\phi_{10}\sigma_0$. The baseline, straight trailing edge is named as $\phi_0\sigma_\infty$ because it has no serration angle but the flow resistance will be infinity due to the solid state.

In Table I, there are five trailing edge devices mainly used in the noise experiments only. These are $\phi_{10}\sigma_0$, $\phi_{10}\sigma_{2.5k}$ (45 ppi reticulated foam), $\phi_{10}\sigma_{10k}$ (Basotect melamine foam), $\phi_{10}\sigma_{41.2k}$ (needle felting foam), and $\phi_{10}\sigma_{153.4k}$ (Armafoam Sound). The four poro-serrated trailing edges ($\phi_{10}\sigma_{2.5k}$, $\phi_{10}\sigma_{10k}$, $\phi_{10}\sigma_{41.2k}$, and $\phi_{10}\sigma_{153.4k}$) are based upon one particular nonflat plate serrated trailing edge geometry, $\phi_{10}\sigma_0$. Therefore they all share the same $2h$, ϕ , and λ/h , which should be *a priori* in the current optimization study of the porous materials. The only difference is that the σ at the sawtooth gaps is not the same because different types of porous materials were used. Another area of study is the near wake flow measurement for $\phi_7\sigma_0$ and $\phi_7\sigma_{8k}$ (Recemat metal foam). Note that noise characteristics for these two trailing edge devices have already been reported in Vathylakis *et al.*¹¹ Likewise, both $\phi_7\sigma_0$ and $\phi_7\sigma_{8k}$ share the same $2h$, ϕ , and λ/h . The values of σ presented in Table I were obtained experimentally from a purposely built system. The experimental procedure in determining the σ will be discussed in Sec. III.

Noise measurements were conducted in an aeroacoustic open jet wind tunnel at Brunel University London. The open jet wind tunnel is situated in a $4 \text{ m} \times 5 \text{ m} \times 3.4 \text{ m}$ anechoic chamber to facilitate free field measurement of the airfoil self-noise. As shown in Fig. 2, the nozzle exit is rectangular with dimensions of 0.10 m (height) \times 0.30 m (width). This wind tunnel can achieve a turbulence intensity of between 0.1% and 0.2% and a maximum jet velocity of about 80 ms^{-1} . The background noise of the wind tunnel facility is well below the self-noise of the quietest airfoil across the whole range of velocity.¹⁹ The range of jet speeds under investigation was between 20 and 60 ms^{-1} , corresponding to Reynolds numbers based on C of 2×10^5 and 6×10^5 , respectively. The airfoil was held by side plates and attached to the nozzle lips. The airfoil was set at 0° angle of attack relative to the jet flow direction.

As shown in Fig. 2, far field noise measurements were made by a single condenser microphone at polar angles of $\Theta = 90^\circ$ at a distance of 1.0 m above the airfoil trailing edge at mid span. Noise data were acquired at a sampling frequency of 44 kHz for 10 s by a 16-bit Analogue-Digital converter from National Instrument. The data were then windowed and the PSD of 1 Hz bandwidth and frequency resolution of 43 Hz was computed from a 1024 point fast Fourier Transform.

To investigate the near wake subjected to the poro-serrated trailing edge, a single hot wire probe ($5 \mu\text{m}$ diameter, 1.25 mm length, DANTEC 55P11) was used to measure the mean and fluctuating velocities of the airfoil wake at an overheat ratio of 1.8. The signals from the hot wire probe were digitized at a sampling frequency of 20 kHz for 120 000 realizations. The hot wire probe was attached to a computer-controlled two-dimensional traverse system with a

TABLE I. Summary of all the trailing edge devices tested in this study. Note that the σ values inside the brackets are extracted from either the commercial suppliers or Geyer *et al.* (Ref. 15).

Symbols	Types of TE	$2h$ (mm)	λ/h	ε (mm)	ϕ ($^\circ$)	σ (kN s m^{-4})
$\phi_0\sigma_\infty$	Baseline, straight	0	0	0	0	∞
$\phi_7\sigma_0$	Nonflat plate serrated	20	0.49	5.7	7	0
$\phi_7\sigma_{8k}$	Poro-serrated	20	0.49	—	7	8.0 (8.2)
$\phi_{10}\sigma_0$	Nonflat plate serrated	20	0.71	5.7	10	0
$\phi_{10}\sigma_{2.5k}$	Poro-serrated	20	0.71	—	10	2.5 (2.0)
$\phi_{10}\sigma_{10k}$	Poro-serrated	20	0.71	—	10	10 (9.8)
$\phi_{10}\sigma_{41.2k}$	Poro-serrated	20	0.71	—	10	41.2 (40.0)
$\phi_{10}\sigma_{153.4k}$	Poro-serrated	20	0.71	—	10	153.4 (112.1)

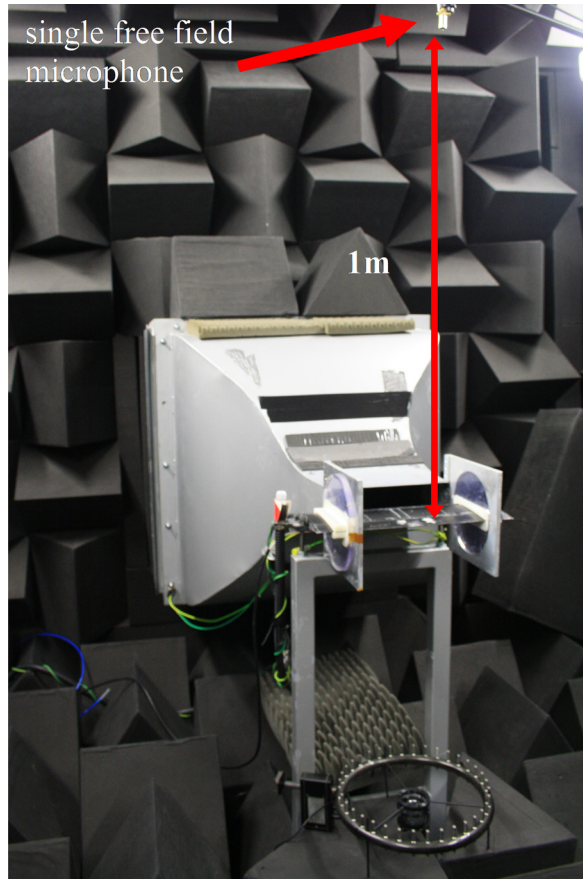


FIG. 2. (Color online) Experimental set up for the airfoil noise tests in an aeroacoustic wind tunnel facility.

resolution of 0.01 mm in both directions. In the current study, the velocity is measured in a $y - z$ plane at $x/C = 1.03$.

III. AIR FLOW RESISTIVITY OF THE POROUS MATERIALS

An important parameter for the poro-serrated trailing edge is the air flow resistivity of the porous materials and how they affect the noise reduction if incorporated into a serrated trailing edge design. The definition of the flow resistivity of a porous sample subjected to through flow relates to the pressure difference ΔP on either side of the sample in question, to the thickness t of the sample and the flow velocity U

$$\sigma = \frac{\Delta P}{Ut}. \quad (1)$$

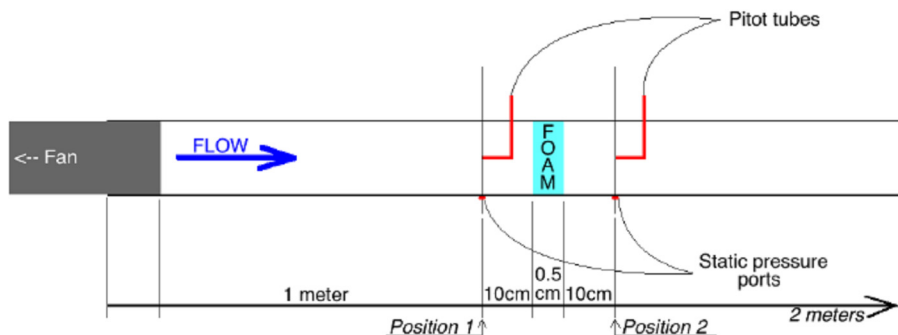


FIG. 3. (Color online) Experimental set up for the measurement of air flow resistivity σ of different porous materials.

Therefore measuring the pressure variation across a porous sample allows one to evaluate the flow resistivity. A simple calibration rig was set up for this purpose. As illustrated in Fig. 3, the calibration rig is a 2 m long and 52 mm inner-diameter Perspex tube along which each porous sample can be inserted. A centrifugal fan is placed at one end of the tube to provide air flow. The position of the porous sample relative to the tube entrance was determined beforehand to ensure that it is placed after the internal flow is fully developed following a tripping at the tube entrance. The first static pressure tap of 0.5 mm diameter (upstream of the porous sample) was drilled at a position along the tube where the flow would be fully developed. Then, a hole that would allow the insertion of a Pitot tube was drilled further along the tube such that the Pitot tube tip and the static pressure tap on the Perspex tube would both be aligned at the same position (Position 1). A traverse of the Pitot tube across the cross-section of the calibration pipe was performed to measure the boundary layer profile. The porous sample was then placed 0.1 m away from that first pressure position. The second static pressure tap was drilled at the same 0.1 m clearance from the aft region of the porous sample (Position 2). All the porous sample thickness was chosen as 5 mm, which is close to the value of the serration bluntness ε . The measured air flow resistivities for the different porous samples are listed in Table I, which cover the range of $2 < \sigma < 150 \text{ kN s m}^{-4}$.

Note that the above setup is slightly different with the standard procedure, such as ISO 9053 (Ref. 20) for measuring the flow resistivity of a porous sample. However, the current setting ensures that a fully developed shear flow enters and exits the porous samples, which would mimic reasonably well the poro-serrated setting where turbulent boundary layers flow across the porous sample from the upper side to the lower side, or vice versa, near the airfoil trailing edge. A Basotect melamine foam sample was tested between 5 and 15 ms^{-1} (in a step of 1 ms^{-1}) inside the calibration pipe. The flow resistivity is found to vary linearly with the velocity at about 0.63% per ms^{-1} . During the aeroacoustic measurement, the transverse flow through each porous material in the poro-serrated trailing edge is expected to be within this velocity range. Therefore, a linear deviation of 0.63% per ms^{-1} for the flow resistivity of the porous samples is considered as acceptable. Note that the measured σ for the porous samples are close to the values provided either by the commercial suppliers of the porous material, or those quoted from Geyer *et al.*¹⁵ which were obtained by the ISO 9053 procedure.

IV. NOISE SPECTRA AT A SINGLE, REPRESENTATIVE VELOCITY

Using a single far field microphone at polar angle of $\Theta = 90^\circ$ at a distance of 1.0 m above the airfoil trailing edge at mid span, the sound pressure level (SPL) produced by the six trailing edges ($\phi_0\sigma_\infty$, $\phi_{10}\sigma_0$, $\phi_{10}\sigma_{2.5k}$, $\phi_{10}\sigma_{10k}$, $\phi_{10}\sigma_{41.2k}$, and $\phi_{10}\sigma_{153.2k}$) are shown in Fig. 4(a) for velocity $U = 40 \text{ ms}^{-1}$. The airfoil with the quietest trailing edge is still capable of radiating a higher noise level than the background noise across the whole frequency range. Figure 4(b) shows the difference in SPL (ΔSPL) between the baseline airfoil with straight trailing edge $\phi_0\sigma_\infty$ and the serrated trailing edges. Therefore a positive ΔSPL represents the noise reduction, and a negative ΔSPL represents the noise increase.

Figures 4(a) and 4(b) demonstrate that trailing edge serration cut into the main body of the airfoil $\phi_{10}\sigma_0$, or with the porous materials filling the gaps between adjacent members of the sawtooth ($\phi_{10}\sigma_{2.5k}$, $\phi_{10}\sigma_{10k}$, $\phi_{10}\sigma_{41.2k}$, and $\phi_{10}\sigma_{153.2k}$), has a substantial effect on the radiated noise spectra compared to the baseline straight trailing edge $\phi_0\sigma_\infty$. For analysis

purpose the acoustic spectra in Fig. 4(b) are divided into four frequency (f) zones. Note that the criterion for the division of these frequency zones is based on the ΔSPL characteristics between $\phi_0\sigma_\infty$ and $\phi_{10}\sigma_0$. Zone I corresponds to a low frequency band at $f \leq 800 \text{ Hz}$, which is just before the occurrence of the bluntness-induced vortex shedding tonal noise. Zone II encompasses the frequency band at $800 \leq f \leq 1500 \text{ Hz}$ where the intense bluntness-induced tonal noise occurs. Zone III encompasses $1500 \leq f \leq 6600 \text{ Hz}$ for $+\Delta\text{SPL}$ (reduction of the turbulent broadband noise). Finally, Zone IV represents the high frequency band at $f \geq 6600 \text{ Hz}$ where the trailing edge is unlikely the dominant noise source, i.e., $\Delta\text{SPL} \approx 0$. Sections IV A–IV D discuss the characteristics and significances of the acoustic spectra at these different frequency zones.

A. Zone I

The acoustic spectra at Zone I are most likely to be contributed by the jet noise, and to a lesser extent, the leading edge interaction noise. When the airfoil has a $\phi_{10}\sigma_0$ nonflat plate serrated trailing edge, $+\Delta\text{SPL}$ in the region of

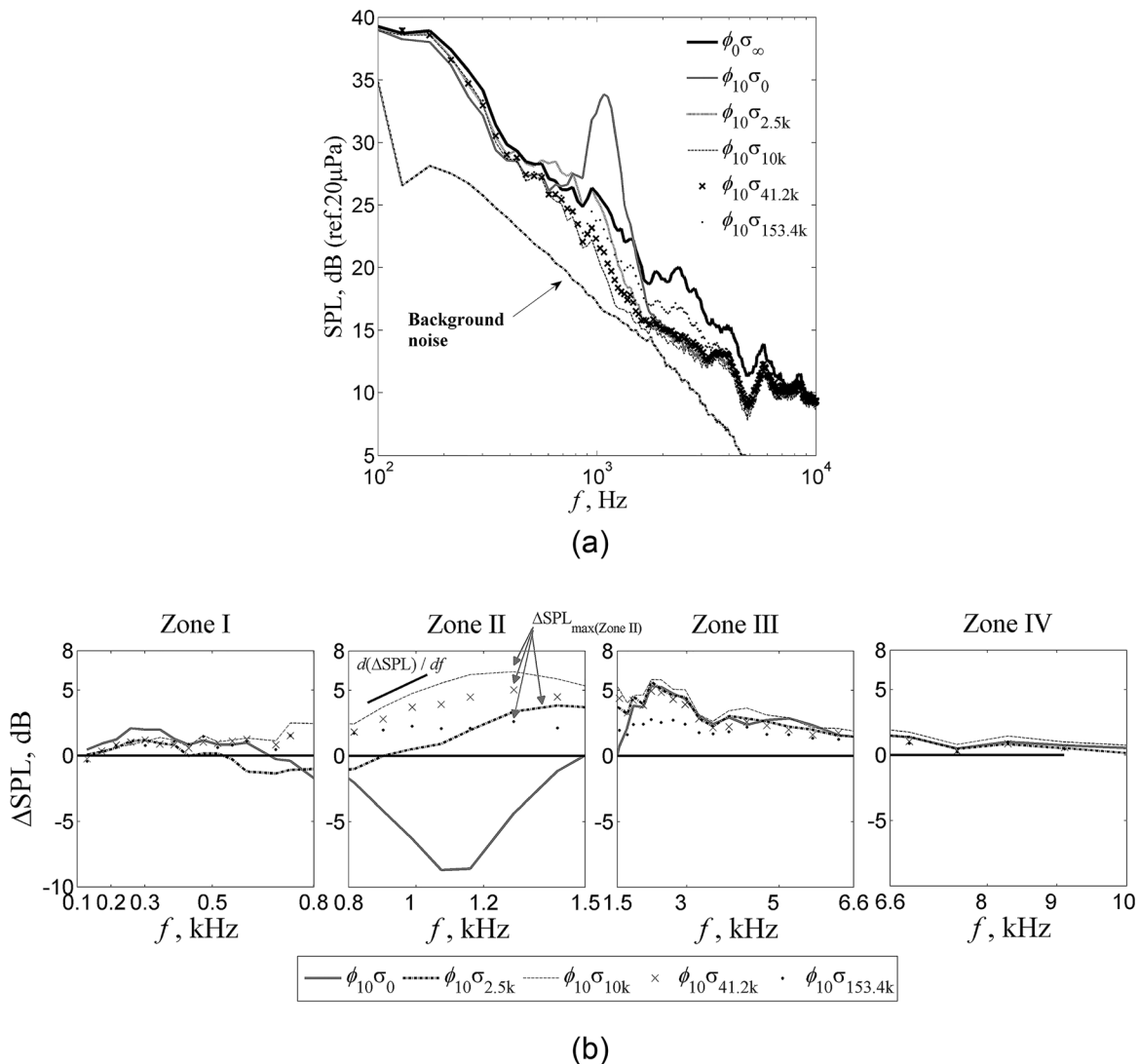


FIG. 4. Comparisons of (a) SPL, dB measured at $U = 40 \text{ ms}^{-1}$ for the baseline straight, nonflat plate serrated, and poro-serrated trailing edges, (b) the corresponding ΔSPL , dB spectra for frequency Zones I, II, III, and IV.

1.5–2 dB is found across almost the entire frequency band within Zone I in Fig. 4(b). Such trend is highly repetitive because several confirmation tests essentially produced the same results. It should be emphasized that the seemingly “noise reduction” achieved by the $\phi_{10}\sigma_0$ nonflat plate serrated trailing edge at low frequency is not contributed by the serration effect *per se*. For this type of trailing edge, the bluntness-induced vortex shedding will be produced at the sawtooth root (see Fig. 13 in Chong *et al.*⁹). While the sawtooth roots produce large scale vortex shedding, the sawtooth tips are not expected to produce one due to the lack of geometrical bluntness. Therefore, the presence of a strong inhomogeneous flow field in the spanwise direction near the trailing edge will cause a distortion of the rear stagnation points across the span of the airfoil. Subsequently, jet flow approaching the airfoil leading edge cannot remain two-dimensional under which the front stagnation points and streamline as a function of z will vary according to the wavelength of the serrated trailing edge. This change in the global flow field will affect the efficiency of the jet-leading edge interaction noise radiation due to the loss in spanwise coherence. As a result, a certain level of $+\Delta\text{SPL}$ can be achieved at this frequency range.

The same trend can also be produced by the $\phi_{10}\sigma_{2.5k}$, $\phi_{10}\sigma_{10k}$, $\phi_{10}\sigma_{41.2k}$, and $\phi_{10}\sigma_{153.2k}$ cases, but with a lower level of ΔSPL (≈ 1 dB). Unlike the $\phi_{10}\sigma_0$ nonflat plate serrated trailing edge, these poro-serrated trailing edges do not possess significant blunt portions at the rear part of the airfoil because the sawtooth gaps have already been filled with porous material. As a result, the physical appearance of the poro-serrated trailing edges will resemble the baseline $\phi_0\sigma_\infty$ straight trailing edge. However, the presence of the porous material can still instigate unsteady transverse flow (in the y -direction) near the trailing edge, thus distorting the rear stagnation points. Although less significant, the similar installation effects as experienced by the airfoil subjected to the $\phi_{10}\sigma_0$ nonflat plate serrated trailing edge will also be present for the other poro-serrated trailing edges.

B. Zone II

The discussion now focuses on frequency Zone II. A prominent feature here is the very large level of narrowband

“tone” produced by the nonflat plate $\phi_{10}\sigma_0$ serration where the peak frequency occurs at about 1 kHz, producing large $\Delta\text{SPL} \approx -9$ dB. An examination of the acoustic spectra produced by the $\phi_{10}\sigma_0$ serration at other velocities indicates that the tone has a clear Strouhal number dependency ($f\varepsilon/U$) of around 0.158, which is shown in Fig. 5(a). The Strouhal number is defined with respect to the bluntness ε (5.7 mm) and flow velocity U . This suggests that the tone noise is associated with the periodic vortex shedding emanated from the sawtooth roots when almost no air flow resistivity exists locally for the $\phi_{10}\sigma_0$ nonflat plate serrated trailing edge. Experimental evidence of the periodic vortex shedding can be found in the flow visualization images in Fig. 13 in Chong *et al.*⁹ The ΔSPL associated with the tonal peak at $U = 30, 40, 50,$ and 60 ms^{-1} are shown in Fig. 5(b).

When porous material is added to the sawtooth gaps of the nonflat plate serration, the local air flow resistivity increases and the trailing edge becomes a porous-serration. As shown in Figs. 4(a) and 4(b), three out of the four poro-serrated trailing edges ($\phi_{10}\sigma_{10k}$, $\phi_{10}\sigma_{41.2k}$, and $\phi_{10}\sigma_{153.2k}$) cease to produce the narrowband tone noise in Zone II. This indicates that vortex shedding is now suppressed by the porous part of the poro-serrated trailing edge. This has been confirmed in the near wake hot wire measurements in the previous study in Vathylakis *et al.*¹¹

The remaining poro-serrated trailing edge of $\phi_{10}\sigma_{2.5k}$, which has the lowest air flow resistivity at the sawtooth gaps, produces a small negative ΔSPL at $500 \leq f \leq 900 \text{ Hz}$, i.e., encompassing both Zone I and Zone II. If one compares the acoustic spectra and ΔSPL between $U = 20$ and 60 ms^{-1} in Fig. 6(a), tone noise can still be observed for the $\phi_{10}\sigma_{2.5k}$ poro-serrated trailing edge. Using the same bluntness $\varepsilon = 5.7 \text{ mm}$, Fig. 5(a) also shows the $f\varepsilon/U$ pertaining to the tone noise produced by the $\phi_{10}\sigma_{2.5k}$ poro-serrated trailing edge. It was found that the reduced frequencies between $U = 30$ and 60 ms^{-1} average at about 0.103. Although it is still demonstrating a Strouhal number dependency, this value is significantly lower than the 0.158 produced by the $\phi_{10}\sigma_0$ nonflat plate serrated trailing edge. From the ΔSPL plot in Fig. 6(b), a moderate level of residual tone can still be radiated by the $\phi_{10}\sigma_{2.5k}$ poro-serrated trailing edge at relatively high velocities. This is different with the $\phi_{10}\sigma_0$ case where a strong level of tone noise can already be produced at low

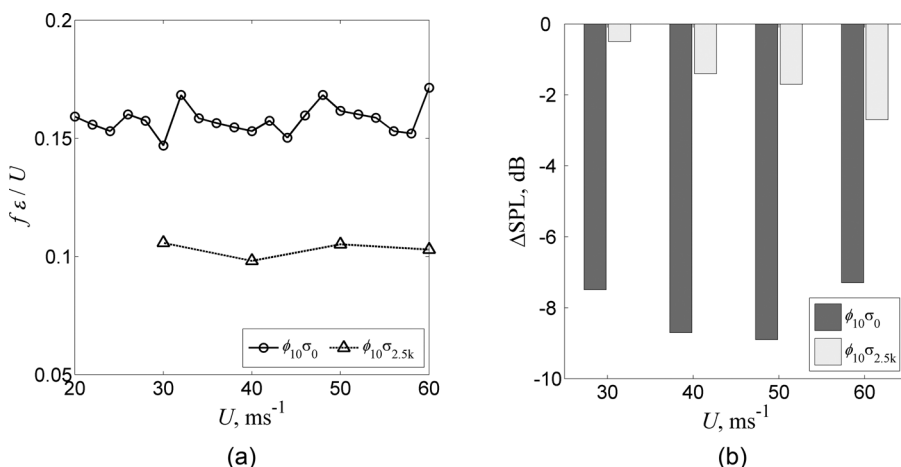


FIG. 5. (a) Distribution of Strouhal numbers ($f\varepsilon/U$) that correspond to the narrowband tonal peak against U , and (b) comparison of the $-\Delta\text{SPL}$ that corresponds to the tonal peak against U .

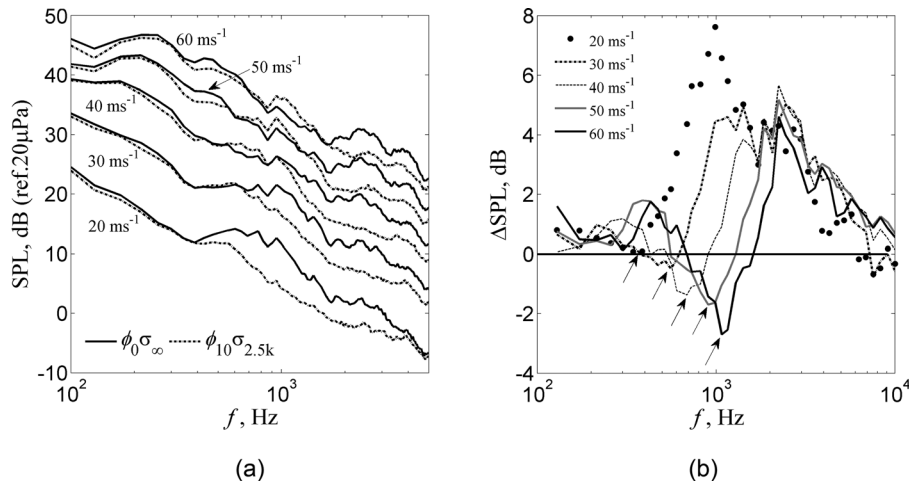


FIG. 6. (a) Comparison of the SPL spectra at different U between $\phi_0\sigma_\infty$ (baseline) and $\phi_{10}\sigma_{2.5k}$ (poro-serrated) trailing edges. (b) ΔSPL produced by the $\phi_{10}\sigma_{2.5k}$ poro-serrated trailing edge at different U .

velocity, as shown in Fig. 5(b). It shows that gradually increasing the σ can reduce both the tone frequency and amplitude of the tone noise. Based on the results in Figs. 5(a) and 5(b), and those already published in Vathylakis *et al.*,¹¹ when $\sigma < 8 \text{ kN s m}^{-4}$, a low level of bluntness-induced tone noise is still present, but with the shedding frequency shifting toward frequency in Zone I. At $\sigma \geq 8 \text{ kN s m}^{-4}$, the vortex shedding can be suppressed effectively and no noticeable tonal characteristic is found in the noise spectra across the velocity range.

Back to Fig. 4(b), another important feature achieved by the poro-serrated trailing edges in Zone II is their ability to significantly reduce the broadband noise, albeit there is also a systematic variation in the maximum level of noise reduction $\Delta\text{SPL}_{\text{max(Zone II)}}$ and the gradient $d(\Delta\text{SPL})/df$ amongst the poro-serrated trailing edges. The gradient $d(\Delta\text{SPL})/df$ is defined as the linear best fit between $f = 800 \text{ Hz}$ and $f \rightarrow \Delta\text{SPL}_{\text{max(Zone II)}}$ [note the linear abscissa in Fig. 4(b)]. As summarized in Table II, the $\phi_{10}\sigma_{10k}$ poro-serrated trailing edge produces the largest levels of both $\Delta\text{SPL}_{\text{max(Zone II)}}$ and $d(\Delta\text{SPL})/df$, followed by $\phi_{10}\sigma_{41.2k}$ and then $\phi_{10}\sigma_{153.4k}$. $\Delta\text{SPL}_{\text{max(Zone II)}}$ for these poro-serrated cases ($\phi_{10}\sigma_{10k}$, $\phi_{10}\sigma_{41.2k}$, and $\phi_{10}\sigma_{153.4k}$) all occur at around $f = 1.26 \text{ kHz}$, and the level of $+\Delta\text{SPL}$ improves as σ reduces.

For the $\phi_{10}\sigma_{2.5k}$ poro-serrated trailing edge, it begins with a negative ΔSPL at $f = 800 \text{ Hz}$ (beginning of frequency Zone II) due to the production of tonal noise in Zone I. Although the $\phi_{10}\sigma_{2.5k}$ poro-serrated trailing edge exhibits a similar level of $d(\Delta\text{SPL})/df$ as the $\phi_{10}\sigma_{10k}$ case, it will always produce a lower level of $+\Delta\text{SPL}$ than other poro-serrated trailing edges with higher σ in Zone II. Moreover, the $\Delta\text{SPL}_{\text{max(Zone II)}}$ produced by the $\phi_{10}\sigma_{2.5k}$ poro-serrated trailing edge occurs at a higher frequency at $f \approx 1.45 \text{ kHz}$.

TABLE II. Summary of all the noise performances for the poro-serrated trailing edges in frequency Zone II.

Poro-serrated trailing edges	$d(\Delta\text{SPL})/df$	$\Delta\text{SPL}_{\text{(max), dB}}$
$\phi_{10}\sigma_{2.5k}$	0.009	3.9
$\phi_{10}\sigma_{10k}$	0.010	6.4
$\phi_{10}\sigma_{41.2k}$	0.007	5.1
$\phi_{10}\sigma_{153.4k}$	0.002	2.7

The poro-serrated trailing edges ($\phi_{10}\sigma_{2.5k}$, $\phi_{10}\sigma_{10k}$, $\phi_{10}\sigma_{41.2k}$, and $\phi_{10}\sigma_{153.2k}$) all share the same serration parameters in $2h$, ϕ , and λ/h , but they have different values of σ . Based on the above observation, the systematic variation in the level of broadband noise reduction among the poro-serrated trailing edges in this frequency zone seems to be predominantly caused by the effect of flow resistivity σ from the porous materials at the sawtooth gaps, where a change of local flow dynamics can further interact with the serration sawtooth to contribute in a broadband noise reduction. This issue will be discussed later.

C. Zone III

As shown in Figs. 4(a) and 4(b), the $\phi_{10}\sigma_0$ nonflat plate serrated, as well as the $\phi_{10}\sigma_{2.5k}$, $\phi_{10}\sigma_{10k}$, $\phi_{10}\sigma_{41.2k}$, and $\phi_{10}\sigma_{153.2k}$ poro-serrated trailing edges all demonstrate that they can achieve a substantial broadband noise reduction in this large frequency zone. It is interesting to note that the vortex shedding, being described so far as an unwanted and adverse flow phenomenon in the frequency Zone II, does not seem to be detrimental to the serration effect on the broadband noise reduction in the frequency Zone III. In the context of nonflat plate serration, it has even been suggested that the presence of transverse flow within the sawtooth gaps is one of the pre-requisites for the manifestation of the serration effect.¹⁴

The first direct comparison between a conventional serrated trailing edge ($\phi_{10}\sigma_0$) and a poro-serrated trailing edge can be made in this frequency zone. The levels in broadband noise reduction in $+\Delta\text{SPL}$ achieved by the $\phi_{10}\sigma_{2.5k}$ and $\phi_{10}\sigma_{10k}$ poro-serrated trailing edges can be up to 1.5 dB higher than the $\phi_{10}\sigma_0$ nonflat plate serrated trailing edge at some frequencies. For the $\phi_{10}\sigma_{41.2k}$ poro-serrated trailing edge, where σ increases to 41.2 kN s m^{-4} , the level of broadband noise reduction starts to dip and has a slightly lower level of $+\Delta\text{SPL}$ than that achieved by the $\phi_{10}\sigma_0$ nonflat plate serrated trailing edge. This implies that the relatively high flow resistivity at the sawtooth gaps of the $\phi_{10}\sigma_{41.2k}$ case begins to interfere negatively with the serration effect at this frequency zone. The $\phi_{10}\sigma_{153.4k}$ poro-serrated trailing edge, which has the largest σ at the sawtooth gaps, can only achieve a moderate $+\Delta\text{SPL}$. The $\phi_{10}\sigma_{153.4k}$ poro-serrated

trailing edge is indeed the lowest performer in the broadband noise reduction among all the trailing edge devices tested here. As σ increases, the porous material used in the sawtooth gaps becomes denser. This would render the poro-serrated trailing edge to gradually become a straight counterpart $\phi_0\sigma_\infty$, thus undermining the serration effect and causing a drop in the performance of broadband noise reduction.

In ascending order, the level of $+\Delta\text{SPL}$ achieved among the trailing edge devices is as follows: $\phi_{10}\sigma_{153.4k}$, $\phi_{10}\sigma_{41.2k}$, $\phi_{10}\sigma_0$, $\phi_{10}\sigma_{2.5k}$, and $\phi_{10}\sigma_{10k}$. Both the serrated ($\phi_{10}\sigma_0$) and poro-serrated ($\phi_{10}\sigma_{2.5k}$, $\phi_{10}\sigma_{10k}$, $\phi_{10}\sigma_{41.2k}$, and $\phi_{10}\sigma_{153.2k}$) trailing edges share the same serration parameters in $2h$, ϕ , and λ/h , but they are different in σ . Therefore, while the main mechanism underpinning the broadband noise reduction is clearly by the serration effect,¹¹ the flow resistivity at

the sawtooth gaps represents another avenue to further improve the noise reduction capability in this frequency zone because the $\phi_{10}\sigma_{2.5k}$ and $\phi_{10}\sigma_{10k}$ poro-serrated trailing edges have been shown to outperform the $\phi_{10}\sigma_0$ serrated trailing edge slightly.

D. Zone IV

This frequency zone marks the decline in the level of $+\Delta\text{SPL}$ achieved by both the serrated and poro-serrated trailing edge devices, where $\Delta\text{SPL} \rightarrow 0$ as the frequency increases. Neither the sawtooth nor the porous material could exert a significant impact on the acoustic spectrum at high frequency because self-noise radiated from the trailing edge by the dipole scattering of turbulent eddies is no longer the major noise source here.

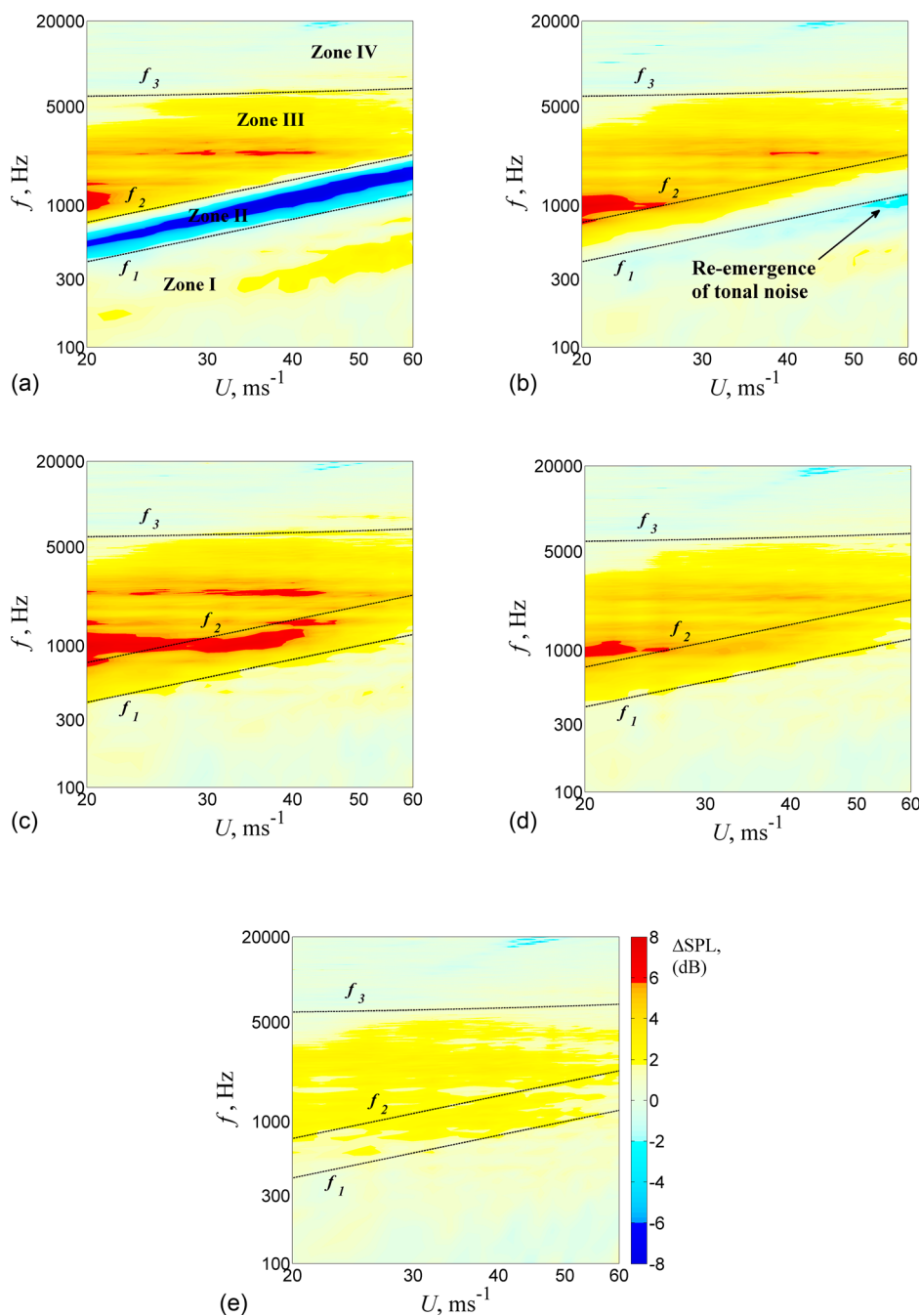


FIG. 7. (Color online) Contours of ΔSPL , dB produced by (a) $\phi_{10}\sigma_0$ non-flat plate serrated trailing edge, and (b) $\phi_{10}\sigma_{2.5k}$, (c) $\phi_{10}\sigma_{10k}$, (d) $\phi_{10}\sigma_{41.2k}$, and (e) $\phi_{10}\sigma_{153.4k}$ poro-serrated trailing edges. The frequency Zones I, II, III, and IV identified in (a) are also applicable to (b)–(e).

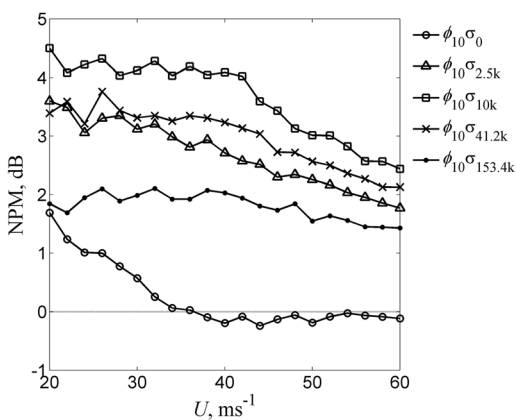
V. NOISE SPECTRA AT OTHER VELOCITIES

This section will examine the noise performance of the serrated and poro-serrated trailing edges at other velocities. Figures 7(a)–7(e) show contour maps of ΔSPL as a function of frequency and mean velocity ($U = 20\text{--}60\text{ ms}^{-1}$) for the $\phi_{10}\sigma_0$, $\phi_{10}\sigma_{2.5\text{k}}$, $\phi_{10}\sigma_{10\text{k}}$, $\phi_{10}\sigma_{41.2\text{k}}$, and $\phi_{10}\sigma_{153.2\text{k}}$, respectively. Note that the velocity resolution in these figures is 2 ms^{-1} . The different frequency Zones I, II, III, and IV identified earlier in Sec. IV are also reproduced here as a function of the velocity, which are defined by

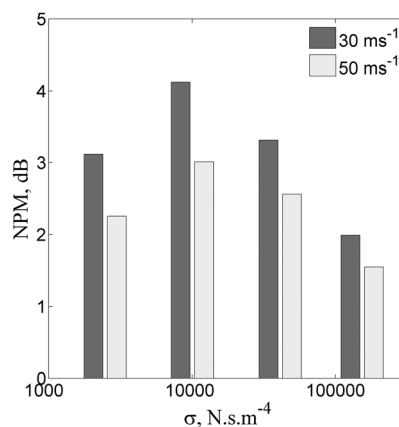
$$\begin{aligned} f_1(U) &= 20 \cdot U^{1.0} \\ f_2(U) &= 38 \cdot U^{1.0} \\ f_3(U) &= 20 \cdot U^{1.0} + 5800. \end{aligned} \quad (2)$$

Both f_1 and f_2 represent the lower and upper limits of the narrowband tone noise in Zone II produced by the $\phi_{10}\sigma_0$ nonflat plate serrated trailing edge. They are both proportional to $U^{1.0}$, which indicates the presence of a Strouhal number relationship. Assuming a characteristic length scale equal to the sawtooth bluntness ε , the corresponding Strouhal numbers are 0.11 and 0.22, respectively. As indicated in Figs. 7(a)–7(e), the variation of f_3 with U is kept at the same velocity scaling to produce an interface that could separate the frequency Zones III and IV reasonably well. The variation of f_3 as a function of U in Eq. (2), which is fitted against the $\phi_{10}\sigma_{10\text{k}}$ poro-serrated trailing edge, is essentially an offset of f_1 with the same gradient. Therefore the frequency difference ($f_3 - f_1$) will be the same across the whole range of U . Note that the same definition of f_3 applies to other trailing edge devices. The reason for choosing the $\phi_{10}\sigma_{10\text{k}}$ poro-serrated trailing edge as the representative one is because it produces the largest frequency bandwidth of $+\Delta\text{SPL}$ amongst others.

In Sec. IV, the $\phi_{10}\sigma_0$ nonflat plate serrated trailing edge at $U = 40\text{ ms}^{-1}$ indicates that noise reduction can be achieved in the frequency Zone I. As shown in Fig. 7(a), noise reduction in Zone I also occurs across a large velocity range especially toward the high velocity end. Significant broadband noise reduction can be found in frequency Zone III. However, a high level of noise increase as a result of the vortex shedding tone features prominently in the frequency Zone II.



(a)



(b)

FIG. 8. Distributions of NPM, dB for frequency Zones (II + III), or $J = (f_1, f_3)$ against (a) U , and (b) flow resistivity σ at the sawtooth gaps.

For all the poro-serrated trailing edges in Figs. 7(b)–7(e), no apparent noise reduction, nor increase, can be observed in the frequency Zone I. Nevertheless, a substantial improvement in the overall noise control performance is demonstrated by the: (1) effective suppression of tonal rungs in Zone II, and (2) significant broadband noise reduction in Zones II and III.

A qualitative examination of Figs. 7(b)–7(e) can easily establish that the level and frequency bandwidth of the broadband noise reduction can be influenced by the flow resistivity σ at the sawtooth gaps of the poro-serrated trailing edges. In order to quantify the difference, an overall Noise Performance Metric (NPM) is defined

$$\text{NPM} = 10 \log_{10} \left(\frac{\int_{f \in J} \bar{p}_{\text{Baseline}}^2 df}{\int_{f \in J} \bar{p}_{\text{Serration}}^2 df} \right), \quad (3)$$

where J is a finite frequency bandwidth that could vary with velocity, and p' is the acoustic pressure fluctuation measured by the microphone. This definition will cause the NPM to be sensitive to the choice of J but nevertheless it is still a useful measure of the noise performance achieved by the serrated trailing edge at a particular U .

Figure 8(a) presents the variations of NPM against U for $\phi_{10}\sigma_0$, $\phi_{10}\sigma_{2.5\text{k}}$, $\phi_{10}\sigma_{10\text{k}}$, $\phi_{10}\sigma_{41.2\text{k}}$, and $\phi_{10}\sigma_{153.2\text{k}}$ when $J = (f_1, f_3)$, which represents the combination of frequency Zones II and III. It can be seen that most of the NPM for the $\phi_{10}\sigma_0$ serrated trailing edge is low and even becoming negative at $U > 36\text{ ms}^{-1}$. This is largely due to the presence of tonal rung in the noise spectrum, where large $-\Delta\text{SPL}$ can be produced [see Fig. 5(b)]. Next, the NPM fluctuates between 2 and 3.5 dB for the $\phi_{10}\sigma_{2.5\text{k}}$ poro-serrated trailing edge over the velocity range investigated here. Despite the rather low level of σ in the $\phi_{10}\sigma_{2.5\text{k}}$ case, the result indicates that: (1) the tonal rung has already been weakened [see Fig. 5(b)], and (2) the overall noise performance is still largely characterized by the reduction in broadband noise. For the $\phi_{10}\sigma_{10\text{k}}$ poro-serrated trailing edge, when σ is larger, the average level of NPM improves to between 2.5 and 4.5 dB. However, a further increase of σ to the level corresponding to the $\phi_{10}\sigma_{41.2\text{k}}$ poro-serration does not result in further

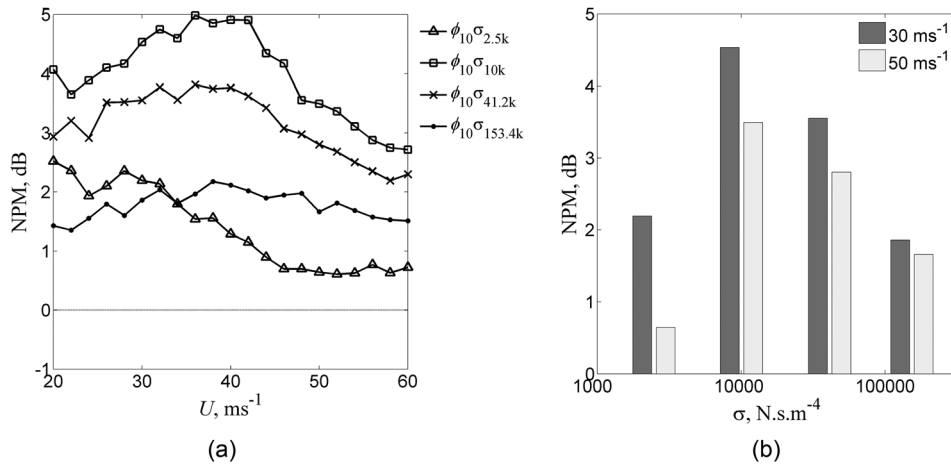


FIG. 9. Distributions of NPM, dB for frequency Zone II only, or $J = (f_1, f_2)$ against (a) U , and (b) flow resistivity σ at the sawtooth gaps.

improvement of the NPM. Instead, the performance is just slightly better than the $\phi_{10}\sigma_{2.5k}$ case. Finally, for the largest σ level tested in this study, the $\phi_{10}\sigma_{153.4k}$ actually achieves the lowest overall performance in NPM between 1.5 and 2 dB amongst other poro-serrated trailing edges. This is caused by the use of dense porous material that renders the trailing edge to become more solid state across the span, thus weakening the serration effect. The results in Fig. 8(a) also show that NPM produced by most of the poro-serrated trailing edges (except the $\phi_{10}\sigma_{153.4k}$ type) reduces as U increases. Figure 8(b) plots the variation of NPM against σ when $J = (f_1, f_3)$ for two velocities. It can be seen that the optimum value of σ at the sawtooth gaps is about 10 kN s m⁻⁴.

Note that the NPM presented above represents a large frequency bandwidth that combines Zones II and III together. Next, the examination will focus on the NPM of Zone II and Zone III, separately. Figure 9(a) presents the variations of NPM against U for the $\phi_{10}\sigma_{2.5k}$, $\phi_{10}\sigma_{10k}$, $\phi_{10}\sigma_{41.2k}$, and $\phi_{10}\sigma_{153.2k}$ when $J = (f_1, f_2)$, i.e., the frequency Zones II only. Note that the NPM for the $\phi_{10}\sigma_0$ nonflat plate serrated trailing edge is not included here because of the expected dominance by the vortex shedding tonal noise. The most notable feature in Fig. 9(a) is that a large variation of NPM is produced among the poro-serrated trailing edges. This indicates that the NPM in this frequency zone is more sensitive to the level of σ

at the sawtooth gaps. In ascending order, the level of NPM achieved among the poro-serrated trailing edges is as follow: $\phi_{10}\sigma_{153.4k}$, $\phi_{10}\sigma_{41.2k}$, and $\phi_{10}\sigma_{10k}$. For the $\phi_{10}\sigma_{2.5k}$ poro-serrated trailing edge, however, its NPM begins with the same category as the $\phi_{10}\sigma_{153.4k}$ counterpart at $U \leq 34$ ms⁻¹, but undergoes a large drop in NPM as U increases up to 46 ms⁻¹. At $U > 46$ ms⁻¹, the NPM does not change much but remains low. The reason that causes the drop in noise performance for the $\phi_{10}\sigma_{2.5k}$ poro-serrated trailing edge at high velocity is due to the re-emergence of a weak vortex shedding at the sawtooth gaps [see Fig. 7(b)]. Figure 9(b) plots the variation of NPM against σ when $J = (f_1, f_2)$. Similarly, the optimum value of σ at the sawtooth gaps is also at 10 kN s m⁻⁴.

Based on the results presented so far, choosing the right porous material at the sawtooth gaps seems to be able to improve the broadband noise reduction. However, a question remains of whether an optimized poro-serrated trailing edge could perform better than the $\phi_{10}\sigma_0$ serrated trailing edge when $\sigma = 0$ at the sawtooth gaps. To provide some hints, examination of the NPM will now focus on the frequency Zone III only, i.e., $J = (f_2, f_3)$. The corresponding NPM against U for all the trailing edge devices are shown in Fig. 10(a). For the $\phi_{10}\sigma_0$ nonflat plate serrated trailing edge, where the influence of tonal rung no longer exists at this frequency zone, the corresponding NPM improves significantly and it has achieved between 2 and 4 dB broadband noise reduction

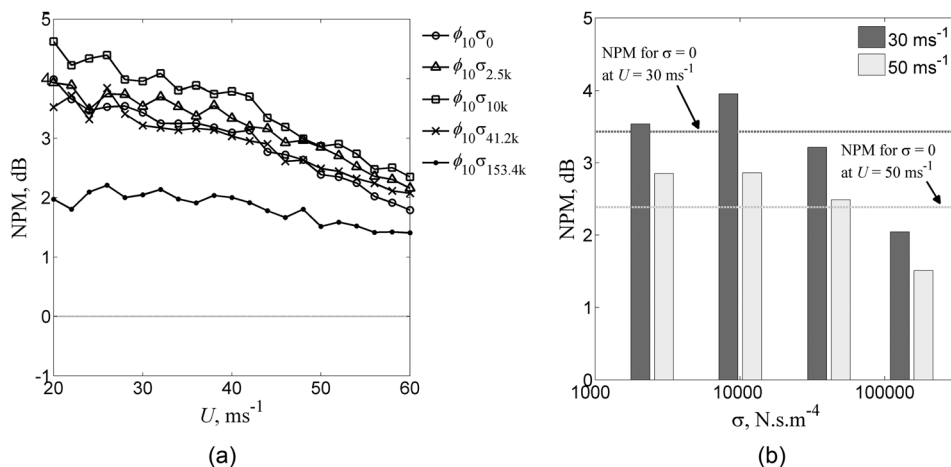


FIG. 10. Distributions of NPM, dB for frequency Zone III only, or $J = (f_2, f_3)$ against (a) U , and (b) flow resistivity σ at the sawtooth gaps.

across the whole velocity range investigated here. The average level of NPM achieved by the $\phi_{10}\sigma_0$ serrated trailing edge is actually quite similar to the $\phi_{10}\sigma_{41.2k}$ poro-serrated trailing edge, where the level of σ at the sawtooth gaps is the second highest. However, the average levels of NPM achieved by the $\phi_{10}\sigma_{2.5k}$ and $\phi_{10}\sigma_{10k}$ poro-serrated trailing edges evidently outperform the $\phi_{10}\sigma_0$ nonflat plate serrated trailing edge. Finally, the NPM for the $\phi_{10}\sigma_{153.4k}$ poro-serrated trailing edge continues to remain the lowest. Figure 10(b) plots the variation of NPM against the σ when $J = (f_2, f_3)$. In this time the NPM for the $\phi_{10}\sigma_0$ nonflat plate serrated trailing edge (where $\sigma = 0$) is indicated in the figure. The results in Fig. 10(b) clearly demonstrate that when a poro-serrated trailing edge has a flow resistivity of $2.5 \leq \sigma \leq 10 \text{ kN s m}^{-4}$ at the sawtooth gaps, the level of broadband noise reduction in NPM it can achieve is up to 0.5 dB higher than that achieved by the $\phi_{10}\sigma_0$ nonflat plate serrated trailing edge.

Generally speaking, the most optimum level of σ at the sawtooth gaps is about 10 kN s m^{-4} for this particular serration geometry of the poro-serrated trailing edge. The performance in NPM then starts to decline when $\sigma > 10 \text{ kN s m}^{-4}$. When $\sigma \rightarrow \infty$, the poro-serrated trailing edge will return to the $\phi_0\sigma_\infty$ baseline trailing edge where the NPM $\rightarrow 0$.

An interesting aspect when $\sigma < 10 \text{ kN s m}^{-4}$, i.e., the $\phi_{10}\sigma_{2.5k}$ poro-serrated trailing edge where $\sigma = 2.5 \text{ kN s m}^{-4}$, is that it has a potential to outperform the $\phi_{10}\sigma_{41.2k}$ counterpart in terms of the level of broadband noise reduction, as demonstrated in Fig. 10(b). However, the $\phi_{10}\sigma_{2.5k}$ poro-serrated trailing edge can also be undermined by the re-emergence of weak vortex shedding at the sawtooth gaps when σ is too low [see Figs. 7(b) and 9(b)]. As a result, when a larger frequency bandwidth is considered, the overall noise performance of the $\phi_{10}\sigma_{2.5k}$ poro-serrated trailing edge

is not as good as the $\phi_{10}\sigma_{41.2k}$ counterpart, as demonstrated in Fig. 8(b).

VI. NEAR WAKE PRODUCED BY THE PORO-SERRATED TRAILING EDGE

This section discusses the results of some of the velocity measurements at the very near wake region produced by the baseline straight, poro-serrated, and nonflat plate serrated trailing edges. The poro-serrated trailing edge used in the wake flow study, denoted here as $\phi_7\sigma_{8k}$, has a narrower serration angle ($\phi = 7^\circ$), but with the same serration amplitude $2h$ as the $\phi_{10}\sigma_0$, $\phi_{10}\sigma_{2.5k}$, $\phi_{10}\sigma_{10k}$, $\phi_{10}\sigma_{41.2k}$, and $\phi_{10}\sigma_{153.4k}$ cases presented previously (See Table I). The porous material used to fill the sawtooth gap of the $\phi_7\sigma_{8k}$ poro-serrated trailing edge is the nickel-chromium foam where the flow resistivity, $\sigma = 8.0 \text{ kN s m}^{-4}$. The corresponding nonflat plate type serrated trailing edge is $\phi_7\sigma_0$. This has exactly the same serration parameters as $\phi_7\sigma_{8k}$, except that $\sigma = 0$ at the sawtooth gaps. As explained in Sec. II, the unsteady velocity was measured by a single hot wire probe traversing in the y - z plane. The streamwise distance of the measurement plane was conducted at $x/C = 1.03$, i.e., about 5 mm from the trailing edge. This distance is usually considered as the very near wake where the viscous sublayer is still well separated from the neighboring inertial sublayer, and the velocity deficit is large at the wake centreline.²¹ The incoming jet velocity was set at $U = 40 \text{ ms}^{-1}$, and the angle of attack was also at 0° . A significant broadband noise reduction can be achieved by both the $\phi_7\sigma_0$ and $\phi_7\sigma_{8k}$ trailing edge devices. The corresponding acoustic spectra had been reported in Vathylakis *et al.*¹¹ [Fig. 5(a)], which will not be repeated here.

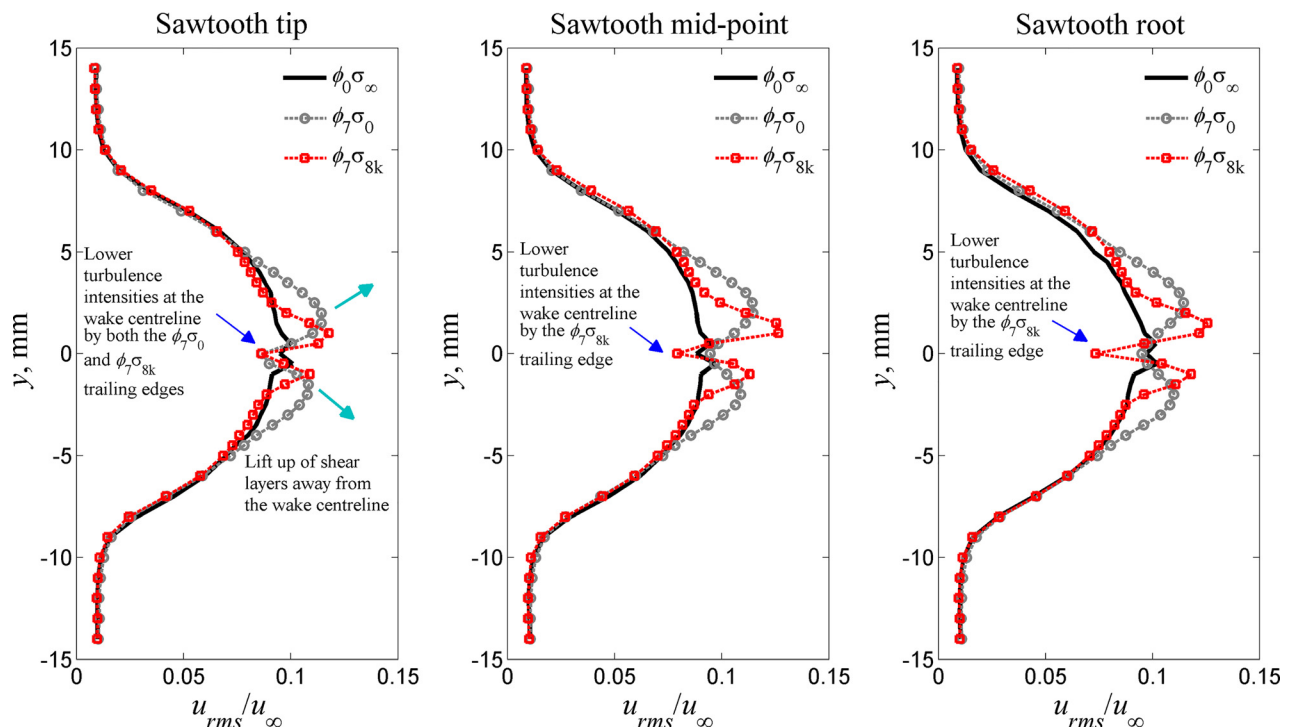


FIG. 11. (Color online) Near wake ($x/C = 1.03$) turbulent velocity profiles at the sawtooth tip, mid-point, and sawtooth root.

Figure 11 shows three fluctuating velocity profiles at different spanwise (z) locations that coincide with the sawtooth tip, mid-point of the oblique edge (referred herein as “mid-point”), and sawtooth root. The shear layers at the sawtooth tip region for the $\phi_7\sigma_0$ and $\phi_7\sigma_{8k}$ trailing edge devices are found to be distinctively different from those produced by the $\phi_0\sigma_\infty$ baseline trailing edge. The results demonstrate that both the shear layers on the upper and lower sides of the poro-serrated trailing edge $\phi_7\sigma_{8k}$, which are mostly originated from the upstream buffer layer, have been lifted away from the wake centreline. Across the sawtooth tip, mid-point, and root, the shear layers also have a higher turbulence intensity level than the shear layers produced by the baseline straight trailing edge, $\phi_0\sigma_\infty$. The presence of flow resistivity at the sawtooth gaps ($\sigma = 8.0 \text{ kN s m}^{-4}$) near the trailing edge should encourage flow “communication” between the upper and lower sides of the airfoil, thereby reducing both the unsteady hydrodynamic pressure difference across the two sides and the effectiveness in noise radiation. Therefore it is reasonable to conjecture that the lifting up of these shear layers for the $\phi_7\sigma_{8k}$ poro-serrated trailing edge is a reaction to the opposing unsteady forces, while the intensified turbulence characteristic of the shear layer is caused by the enhanced turbulent flow mixing, with a possible contribution from the increased surface roughness.

The lifting up of the shear layers is even more pronounced for the nonflat plate serrated trailing edge, $\phi_7\sigma_0$. Because of the virtually zero flow resistance and the resulting large scale vortex shedding at the sawtooth gaps, the shear layers produced by the sawtooth tip, mid-point, and root are universally thicker and further away from the wake centreline than the shear layers produced by the poro-serrated trailing edge $\phi_7\sigma_{8k}$. It is also observed that, for the shear layers developed in the wake flow of the $\phi_7\sigma_0$, their maxima in the turbulence intensities decrease in height from the sawtooth root at $y = \pm 2.3 \text{ mm}$, to the mid-point at $y = \pm 2.0 \text{ mm}$, and finally the sawtooth tip at $y = \pm 1.6 \text{ mm}$.

Geometrically speaking, the sawtooth tips for both the $\phi_7\sigma_0$ and $\phi_7\sigma_{8k}$ trailing edges have exactly the same airfoil cross section as the baseline straight trailing edge $\phi_0\sigma_\infty$. Therefore, without any external influences, the boundary layer and wake developments at any points in the spanwise direction of the baseline trailing edge should produce the same turbulent velocity profile as the sawtooth tip region for the nonflat plate serrated and poro-serrated trailing edge devices. The lack of such correlation in the turbulent velocity profiles between the baseline straight and sawtooth tip, as shown in Fig. 11, suggests that the boundary layer and wake at the sawtooth tip have been mixed with other flow components.

Although the sawtooth tip, mid-point, and root have different geometrical cross-sections for the $\phi_7\sigma_0$ nonflat plate serrated trailing edge, the turbulent velocity profiles produced at these different spanwise locations are quite homogeneous. The same observation also applies to the $\phi_7\sigma_{8k}$ poro-serrated trailing edge. The fact that these turbulent velocity profiles are homogeneous in the spanwise direction suggests the presence of an enhanced spanwise flow mixing mechanism by the porous-serration geometry. The geometrical discontinuities for the sawtooth root,

mid-point, and sawtooth tip occur at $x/C = 0.87, 0.93, \text{ and } 1.00$, respectively. Wake flow is first formed at the sawtooth root region. The shear layers emanated from the sawtooth root will then mix with the boundary layer and shear layers emanated from the oblique side edges, and so on. Such spanwise mixing process will continue until reaching the sawtooth tip.

An important consequence of promoting the lift up of the intensified shear layers near the $\phi_7\sigma_{8k}$ poro-serrated trailing edge is the reduction of turbulence intensity in the near wake centreline. This is manifested in the turbulent velocity profiles in Fig. 11, where the turbulence intensities at $y \approx 0$ pertaining to the sawtooth tip, mid-point, and root regions all exhibit a lower level of turbulence intensity than the $\phi_0\sigma_\infty$ straight trailing edge. It can be assumed that the effectiveness of turbulent broadband noise scattering at the sawtooth tip, oblique edge, and sawtooth root is related to the level of turbulence at the near wall region. The turbulence characteristics at the very near wake, which still retains most of the original characteristics of the upstream turbulent boundary layer, offer an avenue for the study of noise reduction mechanism by the serration. In this case, a weakened turbulent boundary layer noise scattering at the poro-serrated trailing edge is reflected by the low level of turbulence intensity of the near wake centreline across the spanwise direction.

In summary, both the nonflat plate serrated and poro-serrated trailing edges show that: (1) their shear layers are lifted up, where their maxima contain a higher turbulence intensity than the baseline straight trailing edge, (2) the centreline of their near wake profiles contains a lower turbulence intensity than the baseline straight trailing edge (except for the $\phi_7\sigma_0$ case that only occurs at the sawtooth tip), and (3) their turbulent velocity profiles at the sawtooth tip, mid-point, and root regions are generally homogeneous.

VII. CONCLUSIONS

The flow dynamics within the sawtooth gaps, which was subjected to a wide range of flow resistance in this study (including zero flow resistance as the nonflat plate serrated case), can affect the noise performance of an airfoil in the following ways:

For very low flow resistivity at the sawtooth gap (e.g., the $\phi_{10}\sigma_0$ or $\phi_7\sigma_0$ serrated airfoil), the serration effect is enhanced by the oblique cross flow in a direction from the sawtooth root to the tip. The turbulence intensity maxima of the shear layer are lifted away from the wall, while the near wall/wake centreline attain a lower level of turbulence intensity (mainly at the sawtooth tip) than those obtained in a straight trailing edge. Substantial broadband noise reduction can be achieved, presumably due to the weaker noise scattering at the sawtooth tip region. Longitudinal transverse flow (vortex shedding) will be emanated from the sawtooth root in the absence of an effective suppressing mechanism. As a result, large tone noise will be radiated.

For very high flow resistivity at the sawtooth gap (e.g., the $\phi_{10}\sigma_{153.4k}$ poro-serrated airfoil), the serration effect will begin to diminish because it is behaving like a straight trailing edge now. This will lead to a deterioration of the efficiency in the broadband noise reduction. The transverse flow

at the sawtooth gap can be completely suppressed, eventually leading to a large tonal noise reduction.

Finally, for an optimal flow resistivity at the sawtooth gap (e.g., the $\phi_{10}\sigma_{10k}$ poro-serrated airfoil), the serration effect is retained, if not slightly enhanced (see Figs. 4 and 10) where a further 1.5 dB in Δ SPL, or 0.5 dB in NPM higher than the $\phi_{10}\sigma_0$ conventional type serrated airfoil is produced. Multiple broadband noise reduction mechanisms might occur in this case (serration + porous material), but it is more likely that the flow dynamics within the porous material is enhancing the serration, rather than the porous material exerting the “porosity” effect *per se*. The transverse flow at the sawtooth gap can still be completely suppressed to prevent the radiation of vortex shedding tonal noise.

ACKNOWLEDGMENT

The authors are grateful for the financial support from the EPSRC Impact Acceleration Account (IAA) — Readiness in “Poro-serrated trailing edge devices for fan noise reduction applicable to wind turbine and aviation industries”.

¹S. Oerlemans and G. Schepers, “Prediction of wind turbine noise directivity and swish,” 3rd International Meeting on Wind Turbine Noise, Aalborg, Denmark (2009).

²T. Dassen, R. Parchen, J. Bruggeman, and F. Hagg, “Results of a wind tunnel study on the reduction of airfoil self-noise by the application of serrated blade trailing edges,” in *Proceedings of the European Wind Energy Conference* (1996).

³S. Oerlemans, M. Fisher, T. Maeder, and K. Korler, “Reduction of wind turbine noise using optimized airfoils and trailing edge serrations,” *AIAA J.* **47**, 1470–1481 (2009).

⁴L. E. Jones and R. D. Sandberg, “Acoustic and hydrodynamic analysis of the flow around an aerofoil with trailing-edge serrations,” *J. Fluid. Mech.* **706**, 295–322 (2012).

⁵M. Gruber, “Airfoil noise reduction by edge treatments,” Ph.D. thesis, University of Southampton, United Kingdom, 2012.

⁶D. J. Moreau and C. J. Doolan, “Noise-reduction mechanism of a flat-plate serrated trailing edge,” *AIAA J.* **51**, 2513–2522 (2013).

⁷J. Hurault, A. Gupta, E. Sloth, N. C. Nielsen, A. Borgoltz, and P. Ravetta, “Aeroacoustic wind tunnel experiment for serration design optimisation and its application to a wind turbine rotor,” *6th International Meeting on Wind Turbine Noise*, Glasgow, United Kingdom (2015).

⁸T. P. Chong and P. F. Joseph, “An experimental study of airfoil instability tonal noise with trailing edge serrations,” *J. Sound. Vib.* **332**, 6335–6358 (2013).

⁹T. P. Chong, A. Vathylakis, P. F. Joseph, and M. Gruber, “Self-noise produced by an airfoil with nonflat plate trailing-edge serrations,” *AIAA J.* **51**, 2665–2677 (2013).

¹⁰T. P. Chong, P. F. Joseph, and M. Gruber, “Airfoil self-noise reduction by non-flat plate type trailing edge serrations,” *Appl. Acoust.* **74**, 607–613 (2013).

¹¹A. Vathylakis, T. P. Chong, and P. F. Joseph, “Poro-serrated trailing-edge devices for airfoil self-noise reduction,” *AIAA J.* **53**, 3379–3394 (2015).

¹²M. S. Howe, “Noise produced by a sawtooth trailing edge,” *J. Acoust. Soc. Am.* **90**, 482–487 (1991).

¹³B. Lyu, M. Azarpeyvand, and S. Sinayoko, “Prediction of noise from serrated trailing edges,” *J. Fluid Mech.* **793**, 556–588 (2016).

¹⁴T. P. Chong and A. Vathylakis, “On the aeroacoustic and flow structures developed on a flat plate with a serrated sawtooth trailing edge,” *J. Sound Vib.* **354**, 65–90 (2015).

¹⁵T. Geyer, E. Sarradj, and C. Fritzsche, “Measurement on the noise generation at the trailing edge of porous airfoils,” *Exp. Fluids.* **48**, 291–308 (2010).

¹⁶M. Herr, K. S. Rossignol, J. Delfs, M. Mößner, and N. Lippitz, “Specifications of porous materials for low-noise trailing-edge applications,” *20th AIAA/CEAS Aeroacoustic Conference and Exhibit*, AIAA Paper 2014-3041, Atlanta, Georgia (2014).

¹⁷M. R. Fink and D. A. Bailey, “Airframe noise reduction studies and clean-airframe noise investigation,” NASA-CR-159311 (1980).

¹⁸J. M. Jaworski and N. Peake, “Aerodynamic noise from a poroelastic edge with implications for the silent flight of owls,” *J. Fluid Mech.* **723**, 456–479 (2013).

¹⁹A. Vathylakis, T. P. Chong, and J. H. Kim, “Design of a low-noise aeroacoustic wind tunnel facility at Brunel University,” *20th AIAA/CEAS Aeroacoustic Conference and Exhibit*, AIAA Paper 2014-3288, Atlanta, Georgia (2014).

²⁰ISO 9053:1993, “Acoustic—Materials for acoustical applications—Determination of airflow resistance” (International Organization for Standardization, Geneva, Switzerland, 1993).

²¹C. Hah and B. Lakshminarayana, “Measurement and prediction of mean velocity and turbulence structure in the near wake of an airfoil,” *J. Fluid Mech.* **115**, 251–282 (1982).